

Isotopic fingerprints of early Pliocene-like sea surface temperature gradients

George Mason University
Department of Atmospheric,
Oceanic and Earth Sciences

Scott Knapp^a, Natalie J. Burls^a, Sylvia Dee^b, Ran Feng^c, Sarah J. Feakins^d, Tripti Bhattacharya^e
^aGeorge Mason University, ^bRice University, ^cUniversity of Connecticut, ^dUniversity of Southern California, ^eSyracuse University

Introduction

- The Pliocene epoch offers insights into future climate change, with near-modern atmospheric pCO₂ and global mean surface temperature estimated to be 3–4°C above pre-industrial.
- The discrepancy in the hydrological response seen between simulations of future global warming and early Pliocene reconstructions is hypothesized to result from reduced SST gradients in the early Pliocene.
- The interpretation of Pliocene SST proxies is still debated, generating uncertainty in the reduced gradient scenario.
- One avenue toward reducing uncertainty in Pliocene warming patterns is to establish the degree of dynamical consistency between Pliocene SST reconstructions and hydrological cycle reconstructions.
- We seek to identify regions of dynamical consistency using an isotope-enabled GCM, iCAM5, to model the distribution of water isotopes in precipitation.
- We force iCAM5 with climatological SST and sea-ice fields representing modern, abrupt 4xCO₂, late Pliocene and early Pliocene climates.
- The key distinction between the three warming scenarios are their large-scale SST gradients (Fig. 1). The early Pliocene has far weaker SST gradients than both the 4xCO₂ and late Pliocene (Table 1).

Experiment	GMST [°C]	ΔSST [°C] W-E	Max ω Anomaly [Pa/s]	ΔSST [°C] Trop. - Subtrop.	Max Ψ [kg/s]
Pre-industrial	14.13	2.37	0.044	6.61	7.53e10
Abrupt 4xCO ₂	20.15	1.31	0.038	6.13	7.34e10
Early Pliocene	18.99	0.47	0.025	3.99	3.66e10
Late Pliocene	17.85	2.17	0.041	6.23	6.78e10

Table 1. Global mean surface temperature (GMST), ΔSST in the tropical Pacific (8°S–8°N, West 130°E–155°W minus East 155°W–80°W). Max tropical Pacific ω anomaly, calculated as the max value from 10°S–10°N and 130°E–90°W with the mean value (from 10°S–10°N) removed, meant to represent the strength of the Pacific Walker circulation. ΔSST between the tropics (15°N–15°S) and subtropics (20°N–40°N). Maximum value of the atmospheric meridional overturning streamfunction (Ψ), meant to represent the strength of the Hadley cell.

Methods

Model

This study employs the isotope-enabled Community Atmosphere Model (iCAM) version 5.3 (1). The model was run with prescribed climatological monthly mean SST and sea-ice from four scenarios: a preindustrial control (PIC), 4xCO₂ (A4X), early Pliocene (EP)(2) and late Pliocene (LP)(3). In order to create a common control, the three warm scenarios, A4X, LP and EP, were translated into anomaly fields by subtracting their respective coupled climate model PI control monthly climatological SST and sea-ice fields. These anomalies were then added to the PIC monthly climatological SST and sea-ice fields.

Idealized Rayleigh Column

In order to differentiate between changes in δD of water vapor (δD_v) due to thermodynamic changes and those due to changes in atmospheric dynamics, an idealized single-column Rayleigh distillation model (IRC) is employed. This model, described in (4) simulates the effects of Rayleigh distillation on a saturated parcel of air which rises and cools.

Proxy Data Synthesis

Focusing on Africa, we conduct a model-proxy comparison between the available Pliocene-aged estimates of precipitation isotopic composition and each of the four iCAM simulations. We surveyed the literature for plant wax hydrogen isotope reconstructions from marine and lake cores spanning two periods of interest: 5–4 Ma (early Pliocene) and 3.3–3.1 Ma (late Pliocene).

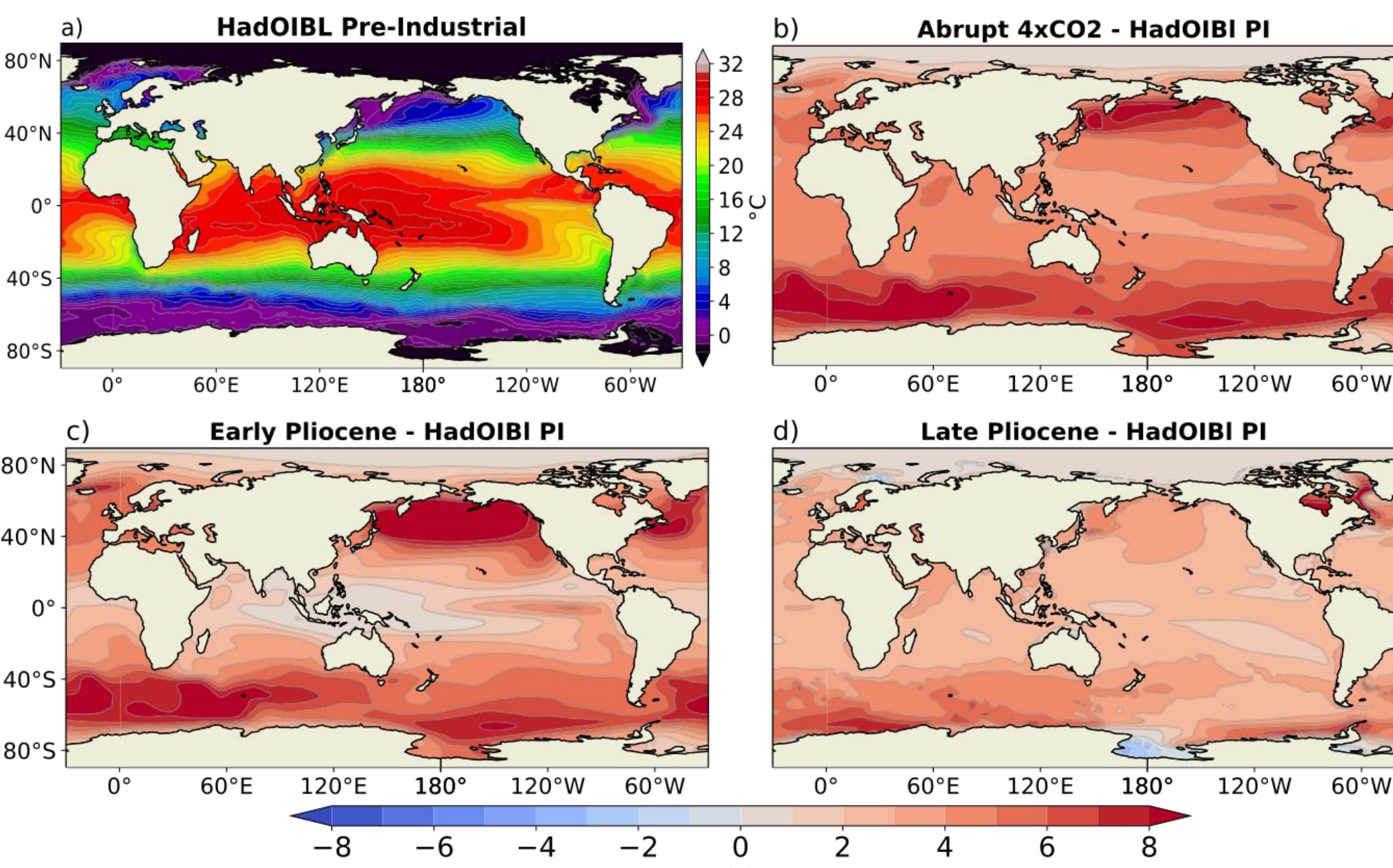


Figure 1. (a) Pre-industrial control (PIC) annual mean SST field. (b-d) Warming scenario annual mean SST minus PIC for (b) the A4X, (c) EP and (d) LP experiments.

Results

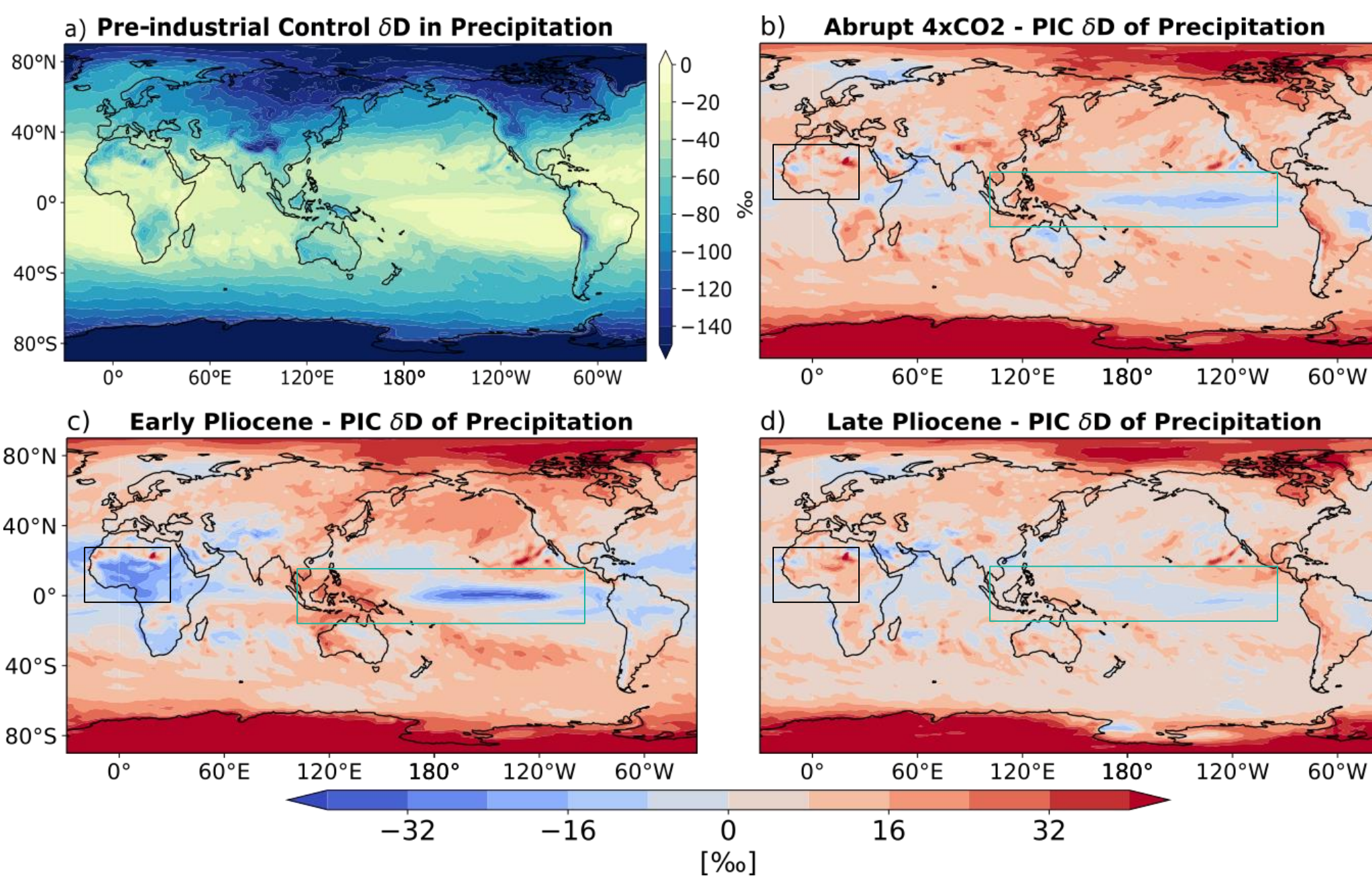


Figure 2. (a) Annual mean δD of precipitation in pre-industrial control (PIC). (b-d) Warming scenario annual mean δD of precipitation minus PIC for (b) the abrupt 4xCO₂, (c) early Pliocene and (d) late Pliocene experiments.

We focus on examining two regions that have the most distinct signal in the weak SST gradient early Pliocene simulation (Fig. 2), as they may be detectable within land-based water isotope proxy records: 1) the equatorial Pacific, and 2) the Sahel region in North Africa. In these regions, the differences simulated in δD_p are consistent between the EP and the other two warm scenarios, despite the differences in global mean surface temperature between A4X and the LP.

The Equatorial Pacific

To examine the relative contributions of the thermodynamic and dynamic effects to the distribution of water isotopes, we adopt the idealized Rayleigh column (IRC) model (4). The IRC identifies the maximum theoretical depletion to the δD of the vapor column due to the temperature profile at each grid (the thermodynamic effect, Fig. 3a and 3b). The residual between the actual vapor content output from the model (Fig. 3, solid lines) and the calculated thermodynamic contribution (Fig 3, dashed lines) is called the dynamic contribution, which represents changes to the δD_v of the column due to the effects of atmospheric circulation on condensation and evaporation.

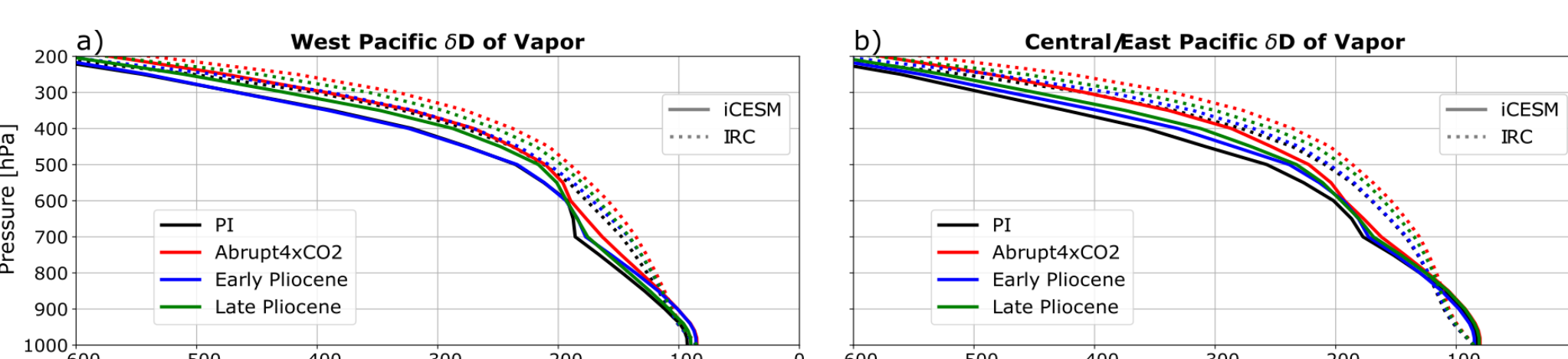


Figure 3. (a) The vertical profile of the δD of vapor in the Idealized Rayleigh Column (IRC; dotted lines) and the iCAM output (solid lines) in the west Pacific (15°S–15°N, 90°E–160°E). (b) As in (a), but for the central/east Pacific (15°S–15°N, 170°E–90°W).

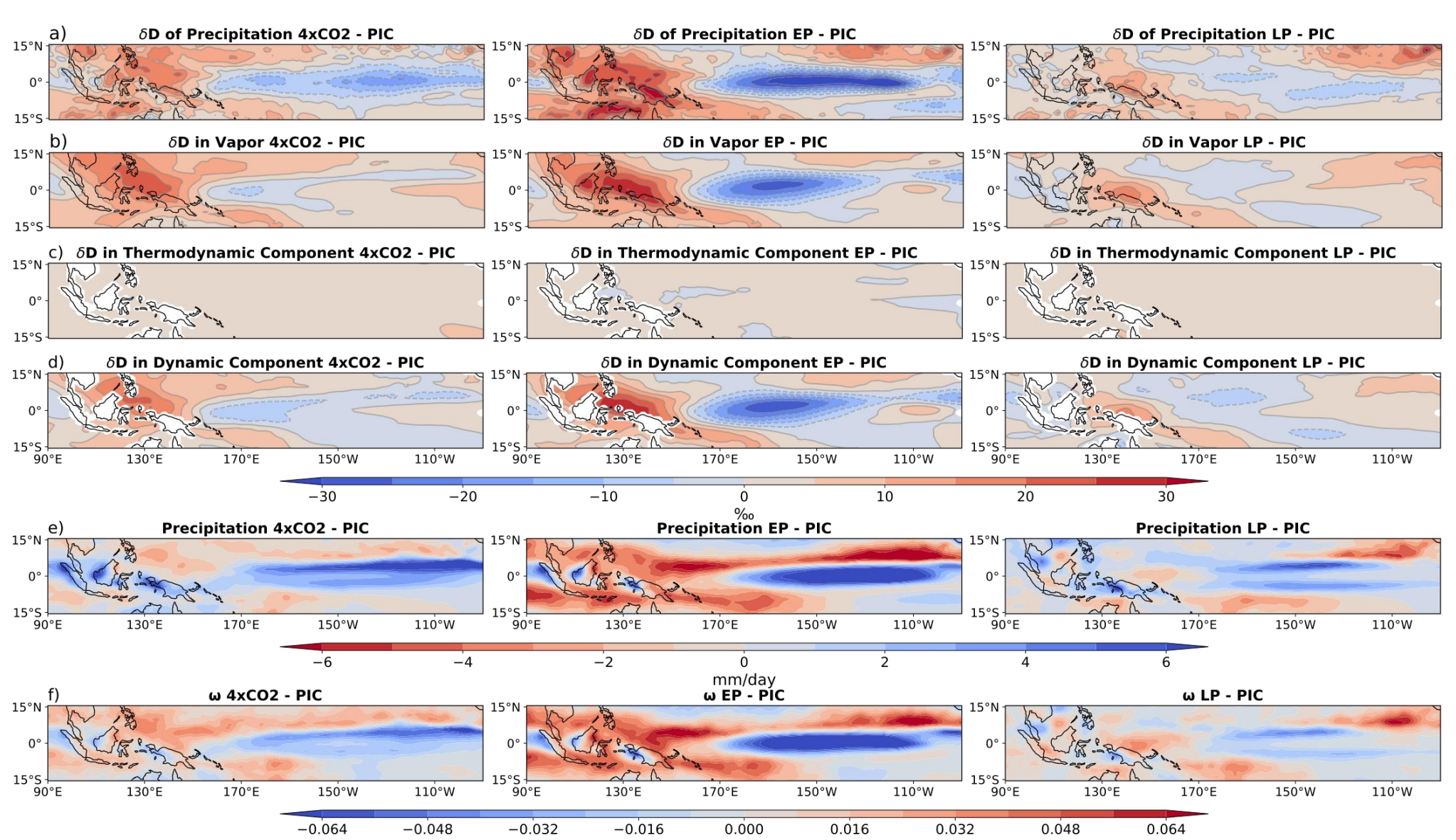


Figure 4. Warming scenario anomalies relative to PIC. (a) δD of precipitation. (b) δD of vapor averaged from 850 hPa to the surface. (c) how much of the δD of vapor is attributed to the thermodynamic component, according to the IRC model. (d) δD of vapor due to the dynamic component, which is the difference between (b) and (c). (e) precipitation in mm/day (f) vertical velocity averaged over 250–500 hPa in Pa/s.

Results

The IRC decomposition of each warming experiment relative to the control (Fig. 4) reveal that the thermodynamic components are nearly homogenous. Most of the spatial structure comes from the dynamic terms. The close match between the differences in dynamic terms and the differences in δD_p support the notion that differences in dynamics are largely responsible for the differences seen in tropical Pacific δD_p in the warming scenario simulations (Fig. 4a & d). Changes in precipitation amount (Fig. 4e) and the strength of deep convection (shown by upper tropospheric vertical velocity, Fig. 4f) represent different aspects of the amount effect, which appear to explain the dynamic component.

The Sahel

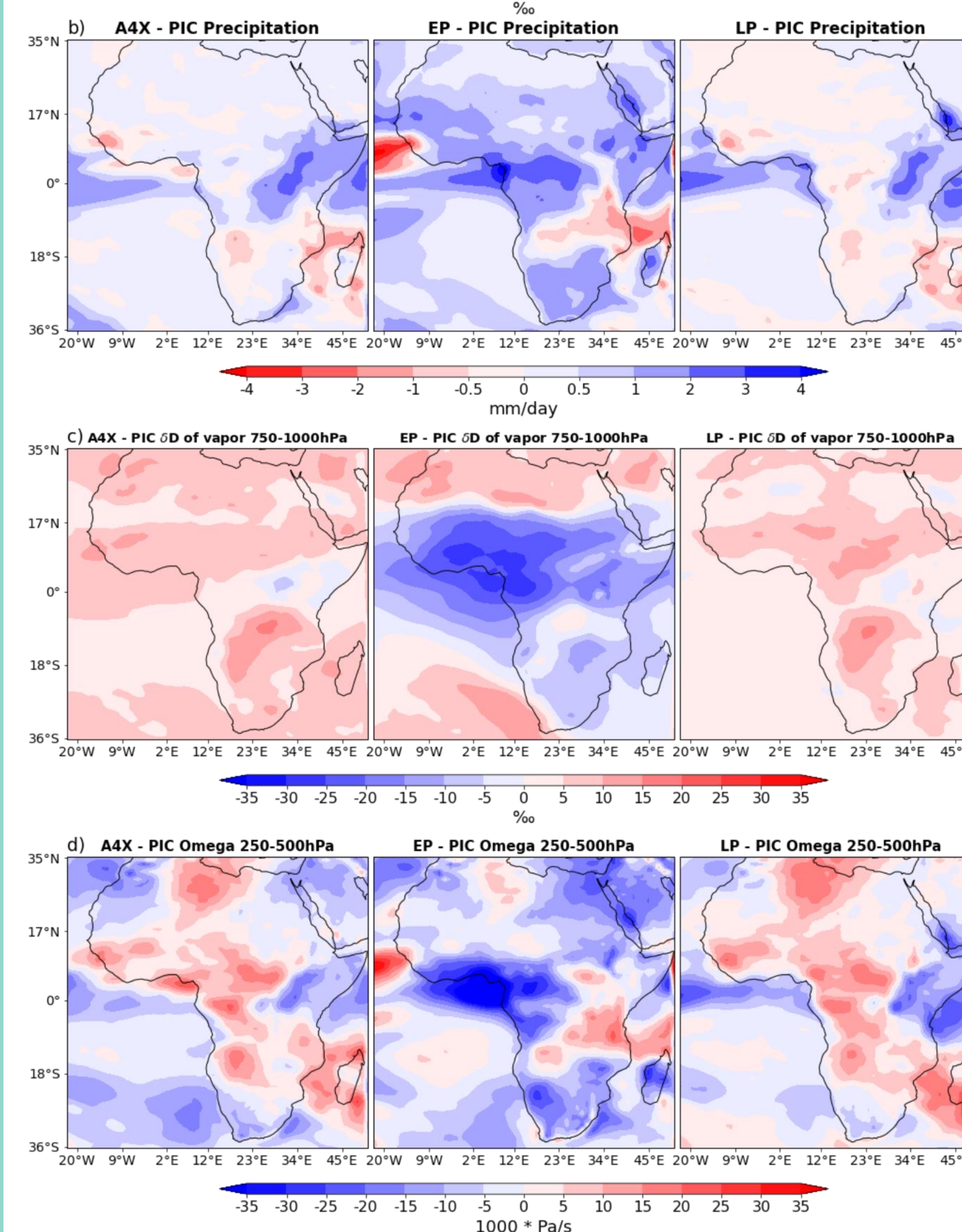
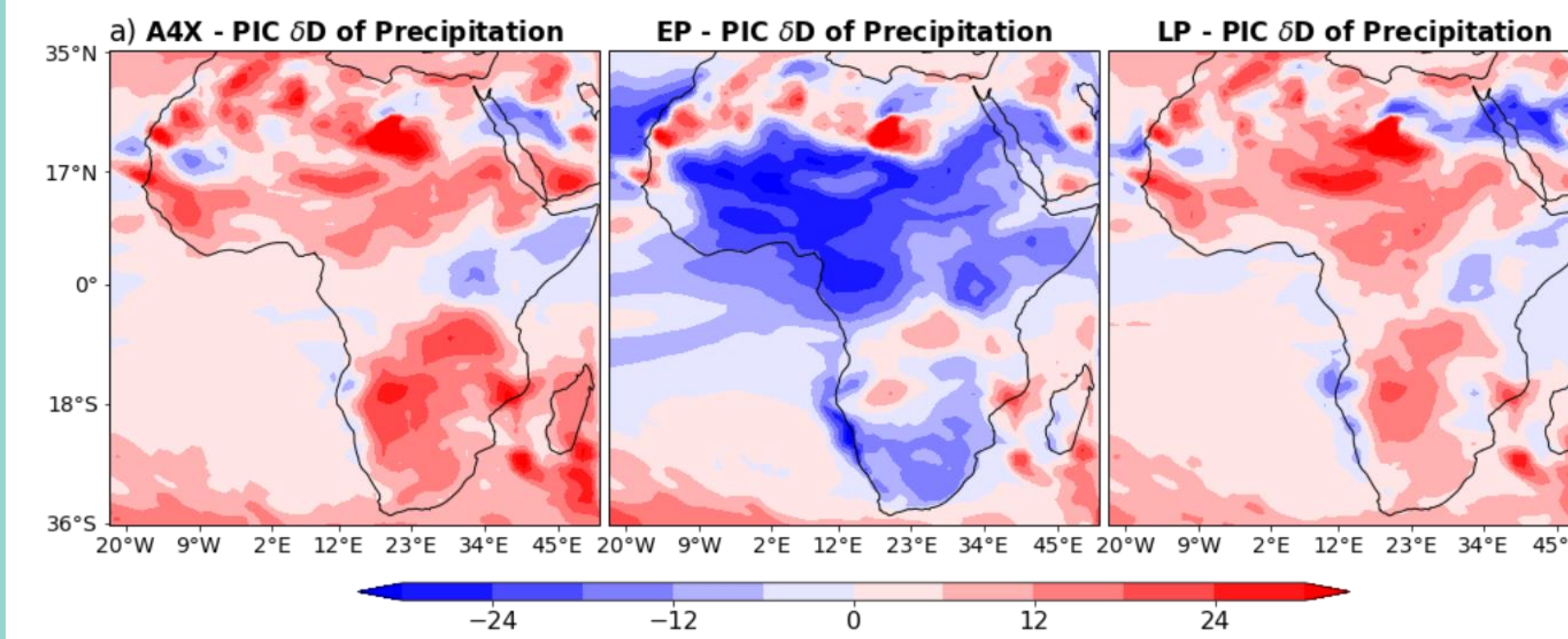


Figure 5. For each experiment, annual means of (a) δD of precipitation, (b) daily precipitation, (c) δD of vapor and wind vectors averaged between 850–1000 hPa, (d) upper Tropospheric (250–500 hPa) vertical velocity

The signal of reduced δD in the EP relative to the LP and A4X is consistent in the Sahel region. The δD fields in Fig. 5a highlight this feature, while also illustrating how similar the A4X and LP are despite their differences in SST forcing (Fig. 1b&d). The anomalous precipitation patterns (Fig. 5b) do not line up with the δD changes as cleanly as in the Pacific, never-the-less there is a general correspondence between the precipitation changes (Fig. 5b) and the δD of precipitation (Fig. 5a) changes across tropical Africa within each simulation. The EP is wetter over most of the African continent relative to the other two warming scenarios, which contributes to the relatively low δD_p. Much of the area of reduced δD_p in the EP is also covered by regions of anomalous deep convection (Fig. 5d), which further contributes to the depletion of vapor and precipitation.

Results

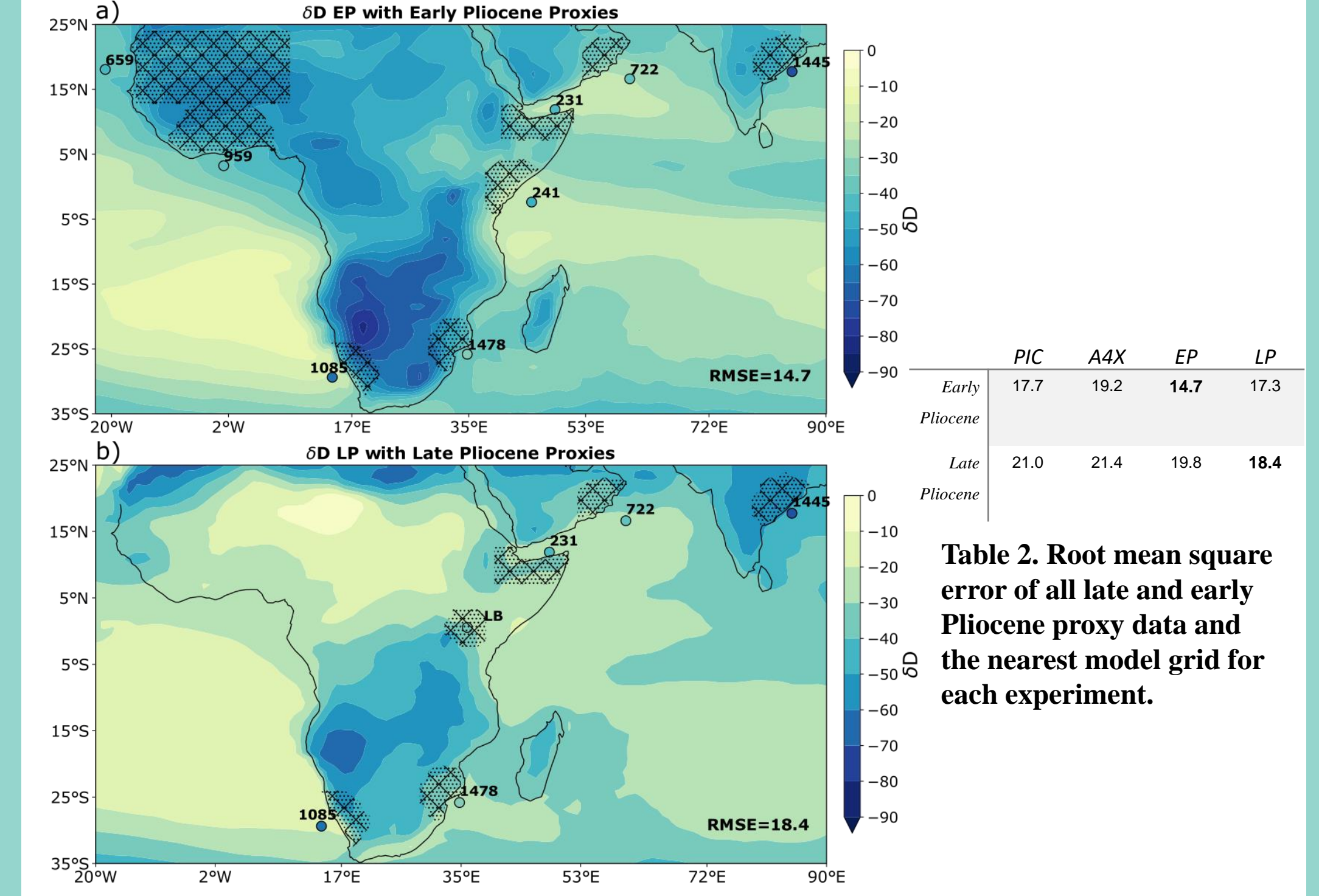


Figure 6. Model-simulated EP (a) and LP (b) δD_p compared to plant-wax proxy based estimates of δD_p (colored circles). Hatched areas represent estimated source regions for each proxy location. RMSE is calculated by comparing the average value in each hatched region to the nearby proxy value.

Comparing the early and late Pliocene δD of precipitation estimates from proxy data to each modeled scenario (Fig. 6) indicates that the EP and LP scenarios have the lowest root-mean-squared-error (RMSE) for their respective proxy data (Table 2). However, a Student's t-test between each pair of squared errors shows that none of the models have errors which are significantly different from one another at the 5% significance level. This emphasizes the need for more precipitation proxy data, so that robust conclusions might be drawn on the degree of the model-proxy agreement.

Conclusion

We have identified two regions where the simulated δD_p change is distinct in response to an early Pliocene SST reconstruction, relative to a late Pliocene reconstruction and a 4x CO₂ scenario. A model-proxy comparison with nine sites in and around Africa indicates that the early and late Pliocene modeled δD_p fields are the best match to their respective proxy data, but more data are needed for a robust test. As more proxy data are produced, further comparisons will provide a way to evaluate the dynamical consistency between Pliocene SST and hydrological cycle reconstructions. Confidence in Pliocene SST reconstructions will allow the community to better use the Pliocene for insight into future changes in the hydrological cycle.

Acknowledgements

This study was supported by the National Science Foundation, via awards AGS-1844380 and OCN-2002448 to N.J.B.; OCE-1903148 and OCE-2029680 to T.B. and OCE-1903650 and OCE-2103055 to R.F. N.J.B. is supported by the Alfred P. Sloan Foundation as a Research Fellow. S.D. is supported by National Aeronautics and Space Administration (NASA) Weather and Atmospheric Dynamics award #80NSSC20K0899. We acknowledge high-performance computing and analysis support from Cheyenne (https://doi.org/10.5065/D6RX99HX) provided by NCAR's Computational and Information Systems Laboratory, sponsored by the NSF. The authors wish to thank Jesse Nusbaumer for assistance with the use of iCAM5.3.

References

- Nusbaumer, J., Wong, T. E., Bardeen, C., & Noone, D. (2017). Evaluating hydrological processes in the Community Atmosphere Model Version 5 (CAM5) using stable isotope ratios of water. *Journal of Advances in Modeling Earth Systems*. https://doi.org/10.1002/2016MS000839
- Burls, N. J., & Fedorov, A. V. (2017). Wetter subtropics in a warmer world: Contrasting past and future hydrological cycles. *Proceedings of the National Academy of Sciences of the United States of America*, 114(49), 12888–12893. https://doi.org/10.1073/pnas.1703421114
- Feng, R., Otto-Bliessner, B. L., Brady, E. C., & Rosenbloom, N. (2020). Increased Climate Response and Earth System Sensitivity From CCSM4 to CESM2 in Mid-Pliocene Simulations. *Journal of Advances in Modeling Earth Systems*, 12(8), e2019MS002033. https://doi.org/10.1029/2019MS002033
- Dee, S. G., Nusbaumer, J., Bailey, A., Russell, J. M., Lee, J.-E., Konecny, B., Buening, N. H., & Noone, D. C. (2018). Tracking the Strength of the Walker Circulation with Stable Isotopes in Water Vapor. *Journal of Geophysical Research: Atmospheres*, 123(14), 7254–7270. https://doi.org/10.1029/2017JD027915